Double reconfigurable intelligent surface-assisted wireless communication system for energy efficiency improvement over weibull fading channels

R. Mahammad Rafi[1] · V. Nivetha[1] · V. Sudha[1]

Abstract

In this paper, we propose a double reconfigurable intelligent surface (RIS)-assisted wireless communication system to improve energy efficiency when a direct link from source to destination is obstructed. First, we model a single RIS-assisted wireless communication system by deploying RIS midway between the source and destination link over the Weibull fading channel. Next, we consider the double-RIS system, in which RIS-1 (R_1) and RIS-2 (R_2) are near the source and destination respectively, with overall reflecting elements in the system equal to the single-RIS system. For both systems, we derive the closed-form expressions for the bounds (lower and upper) of ergodic capacity and exact closed-form expressions for outage probability. The accuracy of the presented theoretical framework is validated through Monte-Carlo simulations. From the comparison, we found that the double-RIS system surpasses the S-RIS system in terms of ergodic capacity and outage probability. Finally, we provide the ergodic capacity and energy efficiency analysis of both systems as a function of spectral efficiency by varying the position of RISs and notice that the double-RIS system with R_1 and R_2 near to source and destination is more energy efficient than the S-RIS system.

Keywords Reconfigurable intelligent surface · Ergodic capacity · Outage probability · Energy efficiency · Weibull fading

1 Introduction

The reconfigurable intelligent surfaces (RISs), built using multiple passive metamaterial reflective elements can convert the dynamic wireless propagation medium into a controllable entity with the assistance of a controller, are one among the prime contenders for developing next-generation wireless communication systems [1]. With huge number of reflective elements whose electromagnetic response (e.g., phase shifts) can be programmable, the RIS can steer the incident signal toward the desired user and provide additional transmission gain when a direct link from source to destination is obstructed [2].

✉ R. Mahammad Rafi
  408119011@nitt.edu

  V. Nivetha
  nivetha@nitt.edu

  V. Sudha
  vsudha@nitt.edu

1 Department of Electronics and Communication Engineering,
   National Institute of Technology, Tiruchirappalli, India

The numerous analyses of single RIS-assisted systems show that the RIS is an energy and spectral efficient technique. The spectrally effective RIS-aided SISO system outperforms both amplify-and-forward (AF) and decode-and-forward (DF) relays in terms of outage probability and offers low bit error rates [3, 4]. It is worth noting that the reconfigurable intelligent surface (RIS) has been demonstrated to have more energy efficiency (EE) than the AF and DF relay [4, 5].

The use of RIS has been investigated extensively in the literature for improving EE in various communication scenarios, such as broadcast and multi-user uplink systems. For example, studies have shown that RIS-assisted broadcast communication can significantly improve EE compared to traditional broadcast communication without RIS [6]. Moreover, the EE-SE tradeoff in the RIS-assisted multi-user uplink system can be optimized by designing the phase shift and covariance matrix [7]. The EE can also be improved by jointly optimizing the active and passive beamforming matrices at the base station and RIS respectively [8]. On the other hand, RIS supports ultra-reliable low latency scenarios with

fewer energy requirements, increases coverage, and minimizes latency [9]. The amalgamation of RIS with multiple access schemes like rate-splitting multiple access and non-orthogonal multiple access (NOMA) will also increase the overall throughput and energy efficiency [10, 11].

However, the works mentioned above focus on a single RIS-aided system. Recently, a plethora of research works has shown that the multi-RIS system achieves higher capacity than a single RIS system [12–15]. Multi-RIS system with a direct link between transceivers outperforms the single RIS-assisted system [12] and outperforms relay-assisted system in terms of average sum rate, but in practical scenarios the direct link between transceivers cannot be guaranteed. In [13], authors show improved outage probability by selecting the RIS with highest instantaneous signal-to-noise ratio (SNR) out of multiple RIS. However, neither the location of RISs nor how to choose a RIS with a high SNR are covered. The authors [14] proposed a distributed on–off approach to increase the energy efficiency of multi-RIS systems which requires reliable channel status information (CSI), which is practically impossible when several RISs are deployed. In [15], authors proposed deep learning and convex optimization-based solution to optimize the energy efficiency of multi-RIS system. But the solution is sub-optimal and the computational complexity and resource allocation will increase with increase in number of RIS. Therefore, EE and resource allocation are crucial when employing a large number of RIS to provide the appropriate Quality of Service (QoS).

Inspired by this, the authors [16] presented a double-RIS-assisted system, with one RIS near the source and another RIS near the destination, to assist the communication between transceivers and show that a double RIS-assisted system achieves higher beamforming gain than a single RIS-assisted system. In addition, a double-RIS-assisted system can also enhance the secrecy of the wireless communication system [17]. Although the prior works on double-RIS-assisted systems have provided remarkable insights, the considered domino patterned system suffers from high path loss due to double reflection, which will deteriorate the received signal power and overall performance. Motivated by the above considerations and to overcome the issue of double reflection in the previous works, we consider a double RIS-assisted system where two RISs will aid communication between transceivers parallelly. Further, we have assumed the practical scenario of direct link blockage between source and destination. The proposed double-RIS system can be used in smart buildings to enhance indoor wireless coverage and improve energy efficiency and it can be used in RIS-assisted-NOMA networks, where the RIS-1 and RIS-2 can assist the near and far users respectively.

1.1 Motivation and contribution

Motivated by the above considerations, in this paper, we provide a comprehensive performance analysis of a double RIS-assisted system in comparison with a single RIS-assisted system. The main contribution of the paper is summarized as follows:

- Analyzed the single RIS and double RIS-assisted systems over Weibull fading channels for the first time.
- We calculate the mean, variance, and second-order moment of received SNR for both systems using the central limit theorem, and thereby closed-form equations for the upper and lower bounds of ergodic capacity and outage probability are obtained.
- Furthermore, the theoretical results are verified through Monte-Carlo simulations, and we provide the comparison between S-RIS and double-RIS systems.
- In addition, by considering circuit dissipated power at the source, RIS, and destination, we present the energy efficiency analysis as a function of spectral efficiency.
- Finally, the impact of RIS locations on the ergodic capacity and energy efficiency of both systems were simulated using the theoretical framework.

1.2 Paper organization

The remainder of the paper is structured as follows. The system model and related channel models of single-RIS and double-RIS-assisted systems are introduced in Sect. 2. The mathematical expressions for the lower, upper bounds of ergodic capacity and outage probability are derived in Sect. 3. In Sect. 4, we present the theoretical and simulation results, and we show the impact of RIS location on ergodic capacity and energy efficiency in Sect. 5. Finally, we draw the conclusions in Sect. 6.

1.3 Notations

Vectors and matrices are denoted using boldface lowercase and boldface uppercase letter respectively. $diag(\boldsymbol{p})$ represents a diagonal matrix with each diagonal element being the corresponding element in $\boldsymbol{p}$, $(.)^T$ stands for transposition, and $\mathrm{Pr}(.)$ defines the probability of an event. The operators $\mathbb{E}[a]$, $\mathbb{V}ar[a]$, and $\mathbb{E}[a^2]$, denote the mean, variance, and second-order moment of random variable a respectively, $\Gamma(.)$ is the Gamma function.

2 System model

2.1 Single RIS-assisted system

We will start with a single RIS-assisted (S-RIS) SISO system in which RIS (R) with N_S reflecting elements is placed in the mid-way between the source (S) and destination (D) as illustrated in Fig. 1. Since the direct link between transceivers is blocked due occlusion, S transmits the signal to D through S-R-D link. Then the signal received at D is given by

$$y_1 = \sqrt{P_S}\Big(\boldsymbol{g}_{RD}^T \boldsymbol{\Phi} \boldsymbol{h}_{SR}\Big)x + n_D, \tag{1}$$

where P_S is the transmit power of S, x is the unit energy signal transmitted by S, and n_D is the additive white Gaussian noise at destination with mean zero and variance σ_D^2, i.e., $n_D \sim \mathcal{CN}\big(0, \sigma_D^2\big)$. The channels of S → R, R → D are denoted by $\boldsymbol{h}_{SR} \in \mathbb{C}^{N \times 1}$, $\boldsymbol{g}_{RD} \in \mathbb{C}^{N \times 1}$ respectively. Also, $\boldsymbol{\Phi} \in \mathbb{C}^{N \times N}$ is the phase shift matrix of R. Under the assumption of unit gain reflection coefficient, $\boldsymbol{\Phi}$ can be expressed as $\boldsymbol{\Phi} = diag\big(e^{\phi_1}, e^{\phi_2}, ..., e^{\phi_N}\big)$ [18]. The elements of $\boldsymbol{h}_{SR}$, $\boldsymbol{h}_{RD}$ are represented as

$$h = d^{-\frac{\eta}{2}} a e^{j\psi}. \tag{2}$$

In Eq. (2) $h \in \{h_i, g_i\}$ denotes the complex fading channel coefficients of S → R, R → D links for the i-th element of R, η is the path loss exponent (PLE) of the corresponding channel. The distances from S to the i-th element of R and i-th element of R to D are denoted as $d \in \{d_{SR_i}, d_{R_iD}\}$, $\psi \in \{\psi_i, \varphi_i\}$ indicates the phase of the corresponding channel and is uniformly distributed over $[-2\pi/\beta, 2\pi/\beta]$. The absolute value of the corresponding channel is denoted by $a \in \{|h_i|, |g_i|\}$ and follows the Weibull distribution with probability density function (PDF) as follows [18]

$$f_A(a) = \frac{\beta}{\Omega} a^{\beta-1} exp\left(-\frac{a^\beta}{\Omega}\right), \tag{3}$$

where $\Omega = \mathbb{E}\big[a^\beta\big] = \left(\frac{\mathbb{E}[a^2]}{\Gamma\left(1+\frac{2}{\beta}\right)}\right)^{\frac{\beta}{2}}$ is the scale parameter, which characterizes the average fading power, and β is the shape parameter that indicates the fading severity. As the value of β decreases, fading severity decreases. The mean, n-th order moment, and variance of the Weibull distribution are $\mathbb{E}[a] = \Omega^{\frac{1}{\beta}}\Gamma\left(1+\frac{1}{\beta}\right)$, $\mathbb{E}[a^n] = \Omega^{\frac{n}{\beta}}\Gamma\left(1+\frac{n}{\beta}\right)$, and $\mathbb{V}ar[a] = \Omega^{\frac{2}{\beta}}\left\{\Gamma\left(1+\frac{2}{\beta}\right) - \left[\Gamma\left(1+\frac{1}{\beta}\right)\right]^2\right\}$ respectively.

We assume S and R have perfect channel state information (CSI). We rely on channel estimation methodologies provided in [19, 20]. Then the maximum SNR at the destination can be written as [21]

$$\gamma_{D,1} = \frac{\left(\sum_{i=1}^{N_S} d_{SR_i}^{-\frac{\eta}{2}} d_{R_iD}^{-\frac{\eta}{2}} |g_i||h_i|\right)^2 P_S}{\sigma_D^2}, \tag{4}$$

similar to [6], we assume that our system belongs to the far-field case, then $d_{SR_i} = d_{SR}$, $d_{R_iD} = d_{RD}$ and Eq. (4). can be written as

$$\gamma_{D,1} = \frac{\left(\sum_{i=1}^{N_S} |g_i||h_i|\right)^2 P_S}{\sigma_D^2 d_{SR}^\eta d_{RD}^\eta} = Z_1^2 \gamma_1. \tag{5}$$

In Eq. (5) $Z_1 = \sum_{i=1}^{N_S} |g_i||h_i|$, $\gamma_1 = \frac{P_S}{\sigma_D^2 d_{SR}^\eta d_{RD}^\eta}$ denotes the transmit SNR.

2.2 Double RIS-assisted system

Now we consider a double-RIS-aided wireless communication system as illustrated in Fig. 2. Since there is no direct link, S transmits the signal to D through RIS-1 (R_1) with $N_1 = N_S/2$ elements is placed near S and RIS-2 (R_2) with $N_2 = N_S/2$ elements is placed near to D. The signal received at the D from both S-R_1-D and S-R_2-D links is given by

$$y_2 = \sqrt{P_S}\Big(\boldsymbol{g}_{R_1D}^T \boldsymbol{\Phi}_1 \boldsymbol{h}_{SR_1} + \boldsymbol{g}_{R_2D}^T \boldsymbol{\Phi}_2 \boldsymbol{h}_{SR_2}\Big)x + n_D, \tag{6}$$

where P_S, x, and n_D are same as S-RIS system. The channels of S → R_1, R_1 → D, S → R_2, and R_2 → D are defined as $\boldsymbol{h}_{SR_1} \in \mathbb{C}^{N_1 \times 1}$, $\boldsymbol{g}_{R_1D} \in \mathbb{C}^{N_1 \times 1}$, $\boldsymbol{h}_{SR_2} \in \mathbb{C}^{N_2 \times 1}$, and $\boldsymbol{g}_{R_2D} \in \mathbb{C}^{N_2 \times 1}$ respectively. Similar to S-RIS system, the phase shift matrices of R_1 and R_2 can be expressed as $\boldsymbol{\Phi}_1 = diag\big(e^{j\phi_{1,1}}, e^{j\phi_{1,2}}, ..., e^{j\phi_{1,N_1}}\big)$ and $\boldsymbol{\Phi}_2 = diag\big(e^{j\phi_{2,1}}, e^{j\phi_{2,2}}, ..., e^{j\phi_{2,N_2}}\big)$ respectively. The elements in $\boldsymbol{h}_{SR_1}$, $\boldsymbol{h}_{R_1D}$, $\boldsymbol{h}_{SR_2}$, and $\boldsymbol{h}_{R_2D}$ are represented as in Eq. (2).

Where the complex fading channel coefficients of S → R_1, R_1 → D, S → R_2, R_2 → D links for the i-th and j-th elements of R_1 and R_2 are denoted by $h \in \{h_{1,i}, g_{1,i}, h_{2,j}, g_{2,j}\}$, η denotes PLE. The distance of corresponding links are denoted as $d \in \{d_{SR_1,i}, d_{R_1,iD}, d_{SR_2,j}, d_{R_2,jD}\}$, where $d_{SR_1,i}$ is the distance from S to i-th element of R_1, $d_{R_1,iD}$ is the distance from j-th element of R_1 to D. Similarly, $d_{SR_2,j}$ is the distance from S to j-th element of R_2 and $d_{R_2,jD}$ is the distance from j-th element of R_2 to D, $\psi \in \{\psi_{1,i}, \varphi_{1,i}, \psi_{2,j}, \varphi_{2,j}\}$ denotes the phase and is uniformly distributed over $[-2\pi/\beta, 2\pi/\beta]$ and $a \in \{|h_{1,i}|, |g_{1,i}|, |h_{2,j}|, |g_{2,j}|\}$ is the absolute value of the corresponding channel and follows the Weibull distribution similar to Eq. (3).

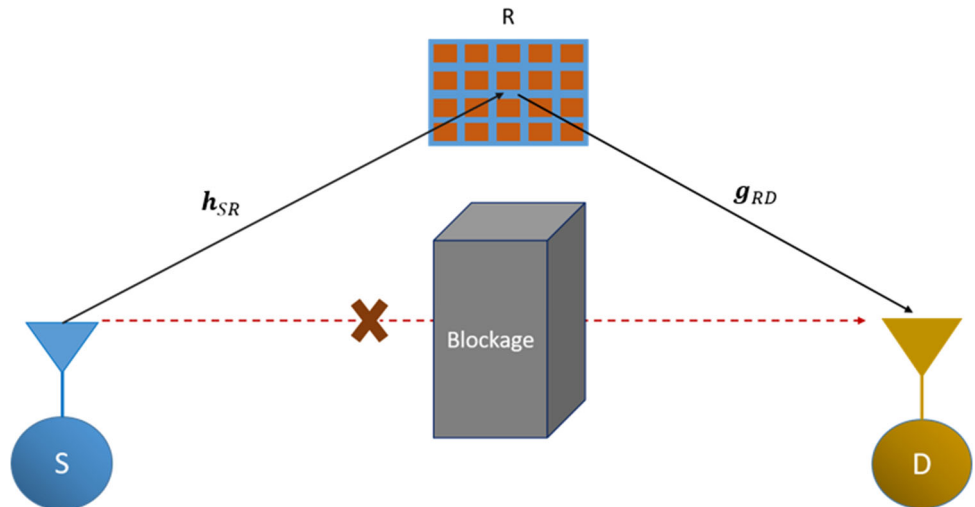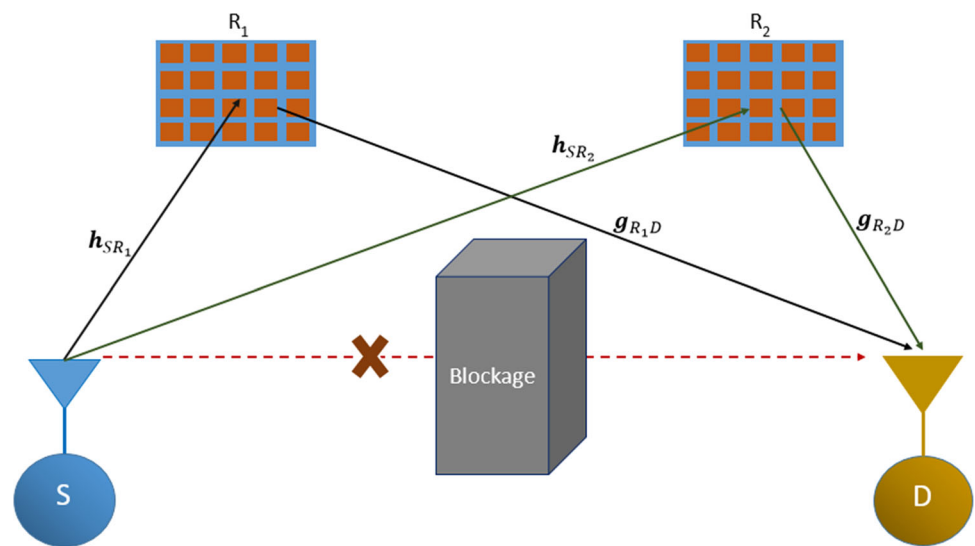**Fig. 1** Single RIS-assisted
wireless communication system

Fig. 2 Double RIS-assisted
wireless communication system

With the assumption of having perfect CSI at both R_1 and R_2 [21], the maximum SNR at the destination in double-RIS system can be obtained as

$$\gamma_{D,2} \tag{7a}$$

$$= \frac{\left(\sum_{i=1}^{N_1} d_{SR_{1,i}}^{-\frac{\eta}{2}} d_{R_{1,i}D}^{-\frac{\eta}{2}} |g_{1,i}| |h_{1,i}| + \sum_{j=1}^{N_2} d_{SR_{2,j}}^{-\frac{\eta}{2}} d_{R_{2,j}D}^{-\frac{\eta}{2}} |g_{2,j}| |h_{2,j}|\right)^2 P_S}{\sigma_D^2},$$

similar to S-RIS system we placed R_1 and R_2 under far-field propagation, hence $d_{SR_{1,i}} = d_{SR_1}$, $d_{R_{1,i}D} = d_{R_1D}$, $d_{SR_{2,j}} = d_{SR_2}$, $d_{R_{2,j}D} = d_{R_2D}$, and by assuming, $N_1 = N_2 = N_D$ where $N_D = N_S/2$ then Eq. 7(a) can be written as

$$\gamma_{D,2}$$

$$= \frac{\left(d_{SR_1}^{-\frac{\eta}{2}} d_{R_1D}^{-\frac{\eta}{2}} \sum_{i=1}^{N_D} |g_{1,i}| |h_{1,i}| + d_{SR_2}^{-\frac{\eta}{2}} d_{R_2D}^{-\frac{\eta}{2}} \sum_{i=1}^{N_D} |g_{2,i}| |h_{2,i}|\right)^2 P_S}{\sigma_D^2},$$

$$\tag{7b}$$

in the double-RIS system, we deployed R_1 and R_2 in such a way that, the product d_{SR_1}, d_{R_1D} is same as the product of d_{SR_2}, d_{R_2D}, i.e., $d_{SR_1}d_{R_1D} = d_{SR_2}d_{R_2D} = d_{tol}$ then,

$$\gamma_{D,2} = \frac{\left(\sum_{i=1}^{N_D} |g_{1,i}| |h_{1,i}| + \sum_{i=1}^{N_D} |g_{2,i}| |h_{2,i}|\right)^2 P_S}{\sigma_D^2 d_{tol}^{\eta}}$$

$$= (A + B)^2 \gamma_2 = Z_2^2 \gamma_2. \tag{8}$$

In Eq. (8) $Z_2 = A + B$, $A = \sum_{i=1}^{N_D} |g_{1,i}| |h_{1,i}|$, $B = \sum_{i=1}^{N_D} |g_{2,i}| |h_{2,i}|$ and $\gamma_2 = \frac{P_S}{\sigma_D^2 d_{tol}^{\eta}}$ denotes the transmit SNR.

3 Performance analysis

This section is devoted to the analysis of ergodic capacity and outage probability of both S-RIS and double-RIS systems.

Before analyzing these metrics first, we need to evaluate mean, variance, second order moment of $\gamma_{D,1}$ and $\gamma_{D,2}$.

3.1 *Mean, second order moment, variance of* $\gamma_{D,1}$

In Eq. (5), the product of independent and identically distributed Weibull random variables $|g_i|$, $|h_i|$ also follows Weibull distribution with mean $\Omega^{\frac{2}{\beta}}(\Gamma(1+1/\beta))^2$ and variance $\Omega^{\frac{4}{\beta}}\left((\Gamma(1+2/\beta))^2 - \Gamma((1+1/\beta))^4\right)$[22, 23]. With the assumption of having a sufficient number of reflecting elements in R, to obey the central limit theorem (CLT), i.e., $N_S \gg 1$, Z_1 follows Gaussian distribution with mean $N_S\Omega^{\frac{2}{\beta}}(\Gamma(1+1/\beta))^2$ and variance $N_S\Omega^{\frac{4}{\beta}}\left((\Gamma(1+2/\beta))^2 - \Gamma((1+1/\beta))^4\right)$. Then $\gamma_{D,1}$ follows a non-central chi-square (*NCCS*) distribution with one degree of freedom [24].

Theorem 1: The mean, variance, and second-order moment of γ_1 can be obtained as

$$\mathbb{E}[\gamma_{D,1}] = N_S\Omega^{\frac{4}{\beta}}\left[(N_S-1)\left(\Gamma\left(1+\frac{1}{\beta}\right)\right)^4 + \left(\Gamma\left(1+\frac{2}{\beta}\right)\right)^2\right]\gamma_1,$$
(9a)

$$\mathbb{E}\left[\gamma_{D,1}{}^2\right] = N_S{}^2\Omega^{\frac{8}{\beta}}\left[\left(N_S{}^2-6N_S+3\right)\left(\left(\Gamma\left(1+\frac{1}{\beta}\right)\right)^8\right)\right.$$
$$+ (6N_S-6)\left(\left(\Gamma\left(1+\frac{2}{\beta}\right)\right)^2\left(\Gamma\left(1+\frac{1}{\beta}\right)\right)^4\right)$$
$$\left. + 3\left(\Gamma\left(1+\frac{2}{\beta}\right)\right)^4\right]\gamma_1^2,$$
(9b)

$$\mathbb{V}ar\left[\gamma_{D,1}\right] = 2N_S{}^2\Omega^{\frac{8}{\beta}}\left[(1-2N_S)\left(\left(\Gamma\left(1+\frac{1}{\beta}\right)\right)^8\right)\right.$$
$$+ (2N_S-2)\left(\left(\Gamma\left(1+\frac{2}{\beta}\right)\right)^2\left(\Gamma\left(1+\frac{1}{\beta}\right)\right)^4\right)$$
$$\left. + \left(\Gamma\left(1+\frac{2}{\beta}\right)\right)^4\right]\gamma_1^2,$$
(9c)

Proof Please refer to Appendix A.

3.2 *Mean, second order moment, variance of* $\gamma_{D,2}$

In Eq. (8) the mean and variance of the product of $|g_{1,i}|,|h_{1,i}|$ and $|g_{2,i}|,|h_{2,i}|$ which are independent and identically distributed Weibull random variables, is given as [22, 23]

$$\mathbb{E}\left[|g_{1,i}|\,|h_{1,i}|\right] = \mathbb{E}\left[|g_{2,i}|\,|h_{2,i}|\right] = \Omega^{\frac{2}{\beta}}\left(\Gamma\left(1+\frac{1}{\beta}\right)\right)^2,$$
(10a)

$$\mathbb{V}ar\left[|g_{1,i}|\,|h_{1,i}|\right] = \mathbb{V}ar\left[|g_{2,i}|\,|h_{2,i}|\right]$$
$$= \Omega^{\frac{4}{\beta}}\left[\left(\Gamma\left(1+\frac{2}{\beta}\right)\right)^2 - \Gamma\left(\left(1+\frac{1}{\beta}\right)\right)^4\right].$$
(10b)

By adopting the similar assumption as in the S-RIS system, i.e., $N_D \gg 1$, A and B follow Gaussian distribution with equal mean and variance as follows,

$$\mathbb{E}[A] = \mathbb{E}[B] = N_D\Omega^{\frac{2}{\beta}}\left(\Gamma\left(1+\frac{1}{\beta}\right)\right)^2,$$
(11a)

$$\mathbb{V}ar[A] = \mathbb{V}ar[B]$$
$$= N_D\Omega^{\frac{4}{\beta}}\left[\left(\Gamma\left(1+\frac{2}{\beta}\right)\right)^2 - \left(\Gamma\left(1+\frac{1}{\beta}\right)\right)^4\right],$$
(11b)

since A and B are independent, their sum Z_2 also follows Gaussian distribution with mean $2N_D\Omega^{\frac{2}{\beta}}(\Gamma(1+1/\beta))^2$ and variance $2N_D\Omega^{\frac{4}{\beta}}[(\Gamma(1+2/\beta))^2 - (\Gamma(1+1/\beta))^4]$. Then $\gamma_{D,2}$ follows NCCS distribution with one degree of freedom [24].

Theorem 2: The mean, variance, and second order moment of $\gamma_{D,2}$ can be obtained as

$$\mathbb{E}[\gamma_{D,2}] = 2N_D\Omega^{\frac{4}{\beta}}\left[(2N_D-1)\left(\left(\Gamma\left(1+\frac{1}{\beta}\right)\right)^4\right)\right.$$
$$\left. + \left(\Gamma\left(1+\frac{2}{\beta}\right)\right)^2\right]\gamma_2,$$
(12a)

$$\mathbb{E}\left[\gamma_{D,2}^2\right]$$
$$= 4N_D^2\Omega^{\frac{8}{\beta}}\left[\begin{array}{l} \left(4N_D^2-12N_D+3\right)\left(\Gamma\left(1+\frac{1}{\beta}\right)\right)^8 \\ + (12N_D-6)\left(\Gamma\left(1+\frac{2}{\beta}\right)\right)^2\left(\Gamma\left(1+\frac{1}{\beta}\right)\right)^4 \\ + 3\left(\Gamma\left(1+\frac{2}{\beta}\right)\right)^4 \end{array}\right]\gamma_2^2,$$
(12b)

$$\mathbb{V}ar\left[\gamma_{D,2}\right]$$
$$= 8N_D^2\Omega^{\frac{8}{\beta}}\left[\begin{array}{l} (1-4N_D)\left(\Gamma\left(1+\frac{1}{\beta}\right)\right)^8 \\ + (4N_D-2)\left(\Gamma\left(1+\frac{2}{\beta}\right)\right)^2\left(\Gamma\left(1+\frac{1}{\beta}\right)\right)^4 \\ + \left(\Gamma\left(1+\frac{2}{\beta}\right)\right)^4 \end{array}\right]\gamma_2^2,$$
(12c)

Proof Please refer to Appendix A.

3.3 Ergodic capacity

The ergodic capacity of both systems is expressed as $C_n = \mathbb{E}\big[\log_2(1+\gamma_{D,n})\big]$, while $n = 1$ and $n = 2$ denotes the S-RIS and double-RIS system respectively. As we mentioned

$$C_{ub_2} = \log_2\left(1 + \gamma_2 2N_D\Omega^{\frac{4}{\beta}}\left[\begin{array}{l}(2N_D-1)\left(\left(\Gamma\left(1+\frac{1}{\beta}\right)\right)^4\right)\\ +\left(\Gamma\left(1+\frac{2}{\beta}\right)\right)^2\end{array}\right]\right),$$

(17)

$$C_{lb_2} = \log_2\left(1 + \frac{\gamma_2\left[2N_D\Omega^{\frac{4}{\beta}}\left[(2N_D-1)\left(\left(\Gamma\left(1+\frac{1}{\beta}\right)\right)^4\right)+\left(\Gamma\left(1+\frac{2}{\beta}\right)\right)^2\right]\right]^3}{4N_D{}^2\Omega^{\frac{8}{\beta}}\left[\left(4N_D{}^2-12N_D+3\right)\left(\Gamma\left(1+\frac{1}{\beta}\right)\right)^8+(12N_D-6)\left(\Gamma\left(1+\frac{2}{\beta}\right)\right)^2\left(\Gamma\left(1+\frac{1}{\beta}\right)\right)^4+3\left(\Gamma\left(1+\frac{2}{\beta}\right)\right)^4\right]}\right).$$

(18)

in earlier, $\gamma_{D,n}$ follows NCCS distribution with one degree of freedom and whose cumulative distribution is mathematically intractable, hence it is difficult to characterize the exact ergodic capacity. Therefore, by utilizing Jensen's inequality, we provide upper and lower bounds of ergodic capacity as [25],

$$C_{lb_n} \le C \le C_{ub_n}.$$

(13)

In Eq. (13), C_{lb} and C_{ub} are defined as [26],

$$C_{ub_n} = \log_2\big(1 + \mathbb{E}[\gamma_{D,n}]\big),$$

(14a)

$$C_{lb_n} = \log_2\left(1 + \frac{\mathbb{E}[\gamma_{D,n}]^3}{\mathbb{E}[\gamma_{D,n}]^2}\right),$$

(14b)

by substituting mean and second order moments of $\gamma_{D,1}$ in Eq. 14(a) and Eq. 14(b) the closed-form expressions to compute C_{ub_1} and C_{lb_1} for the S-RIS containing only elementary functions are given as

$$C_{ub_1} = \log_2\left(1 + \gamma_1 N_S\Omega^{\frac{4}{\beta}}\left[(N_S-1)\left(\Gamma\left(1+\frac{1}{\beta}\right)\right)^4\right.\right.$$
$$\left.\left.+\left(\Gamma\left(1+\frac{2}{\beta}\right)\right)^2\right]\right),$$

(15)

3.4 Outage probability

In this section, we derive the outage probability of S-RIS and double-RIS system, which is defined as the probability that the received SNR falls below a specified threshold γ_{th} [9], i.e.

$$P_{out} = \Pr(\gamma_{D,n} < \gamma_{th}),$$

(19)

or equivalently

$$P_{out} = F_{\gamma_{D,n}}(\gamma_{th}).$$

(20)

As we mentioned in the previous section, γ_n follows NCCS distribution, and by using the cumulative distribution function of $\gamma_{D,n}$ the outage probability is expressed as [9]

$$P_{o,n} = \Pr(\gamma_{D,n} < \gamma_{th}) = 1 - Q_{\frac{1}{2}}\left(\sqrt{\frac{\lambda_n}{\sigma_n{}^2}}, \sqrt{\frac{\gamma_{th}}{\gamma_{D,n}^2\sigma_n{}^2}}\right),$$

(21)

in Eq. (21) $Q_{\frac{1}{2}}(x, y)$ is the Generalized Marcum Q-function with fractional order $1/2$ and can be expressed as [27],

$$Q_{\frac{1}{2}}(x, y) = Q(y - x) + Q(y + x),$$

(22)

$$C_{lb_1} = \log_2\left(1 + \frac{\gamma_1\left(N_S\Omega^{\frac{4}{\beta}}\left[(N_S-1)\left(\Gamma\left(1+\frac{1}{\beta}\right)\right)^4+\left(\Gamma\left(1+\frac{2}{\beta}\right)\right)^2\right]\right)^3}{N_S{}^2\Omega^{\frac{8}{\beta}}\left[\left(N_S{}^2-6N_S+3\right)\left(\Gamma\left(1+\frac{1}{\beta}\right)\right)^8+(6N_S-6)\left(\Gamma\left(1+\frac{2}{\beta}\right)\right)^2\left(\Gamma\left(1+\frac{1}{\beta}\right)\right)^4+3\left(\Gamma\left(1+\frac{2}{\beta}\right)\right)^4\right]}\right).$$

(16)

Similarly, by substituting mean and second order moments of $\gamma_{D,2}$ in Eqs. 14(a) and 14(b) the closed-form expressions to compute C_{ub_2} and C_{lb_2} for the double-RIS containing only elementary functions are given as

by exploiting Eq. (22), the closed-form expression to evaluate outage probability for the S-RIS and double-RIS system are given as

Table 1 Simulation parameters

Parameter	Default values
S → D distance, d_{SD} (m)	200
RIS position in S-RIS system (x_R, y_R) (m)	(100, 10)
Position of R_1 in double-RIS system (x_{R_1}, y_{R_1}) (m)	(5,10)
Position of R_2 in double-RIS system (x_{R_2}, y_{R_2}) (m)	(195,10)
Carrier frequency, f_c (GHz) [12]	3
Power Dissipated at the i-th RIS element, P_i (mW) [12]	7.8
Circuit Dissipated Power at S, P_c^S(dBm) [12]	10
Circuit Dissipated Power at D, P_c^D (dBm) [12]	10
Transmission Bandwidth, BW_T (MHz) [12]	10
Noise Figure, NF (dB)	10
Noise power spectrum density, N_0 (dBm/Hz) [12]	-174
Noise power at destination, $\sigma_D^2 = N_0 + 10\log(BW_T) + NF$, (dBm)	-94
Path loss Exponent,η	3
Path loss at reference distance $d_0 = 1$ m (dB)	-42

$$P_{o,n} = 1 - \left(Q\left(\sqrt{\frac{\gamma_{th}}{\gamma_{D,n}^2 \sigma_n^2}} - \sqrt{\frac{\lambda_{Z_n}}{\sigma_{Z_n}^2}} \right) + Q\left(\sqrt{\frac{\gamma_{th}}{\gamma_{D,n}^2 \sigma_n^2}} + \sqrt{\frac{\lambda_{Z_n}}{\sigma_{Z_n}^2}} \right) \right),$$
(23)

where $\lambda_{Z_1} = N_S^2 \Omega^{\frac{4}{\beta}} (\Gamma(1 + 1/\beta))^4$, $\sigma_{Z_1}^2 = N_S \Omega^{\frac{4}{\beta}} ((\Gamma(1 + 2/\beta))^2 - \Gamma((1 + 1/\beta))^4)$ for S-RIS system and $\lambda_{Z_2} = 4N_D^2 \Omega^{\frac{4}{\beta}} (\Gamma(1 + 1/\beta))^4$, $\sigma_{Z_2}^2 = 2N_D \Omega^{\frac{4}{\beta}} [(\Gamma(1 + 2/\beta))^2 - (\Gamma(1 + 1/\beta))^4]$ for double RIS-system.

4 Simulation results

In this section, we present the simulation results of S-RIS and double-RIS systems to verify the analytical framework presented in the preceding sections. In addition, we compare both systems in terms ergodic capacity, outage probability and energy efficiency by varying the location RISs. To have a fair comparison, we consider an equal number of reflecting elements in both systems, i.e., $N_S = 2N_D = N$, outage threshold SNR $\gamma_{th} = 10$ dB. In addition, the set of parameters given in Table 1 are used in the simulations.

Figure 3 illustrates the ergodic capacity of the S-RIS system with the varying number of reflecting elements N, Weibull shape parameter $\beta = 1$, and scale parameter $\Omega = 1$. The figure shows that, for a fixed N as the transmit power P_S increases, the ergodic capacity of the system also increases.
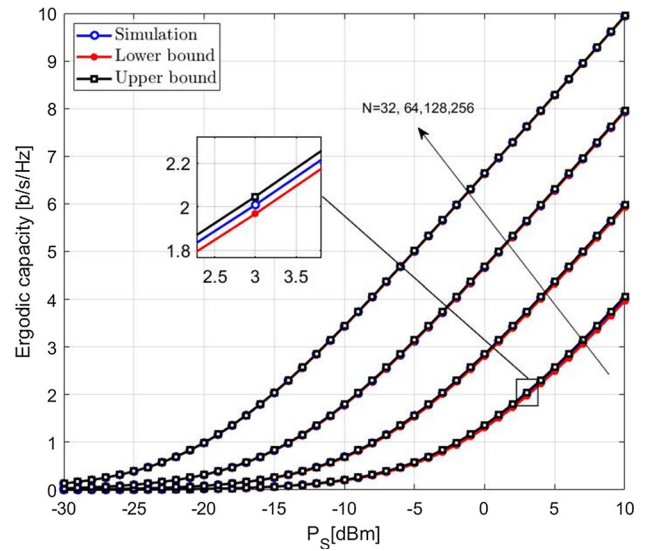

Fig. 3 Simulated Ergodic Capacity, upper and lower bounds of S-RIS system versus transmit power of the source (P_S) for varying N, $\beta = 1$, $\Omega = 1$
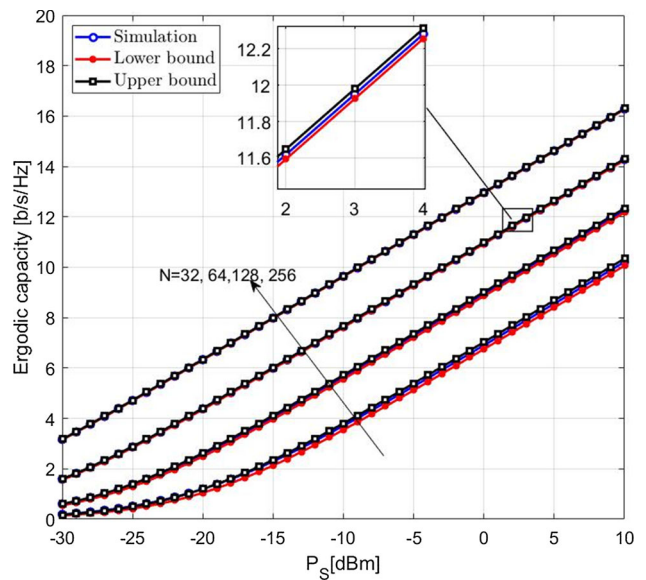

Fig. 4 Simulated Ergodic Capacity, upper and lower bounds of double-RIS system versus transmit power of the source (P_S) for varying N, $\beta = 1$ and $\Omega = 1$

This is because higher transmit power results in a stronger signal at the receiver, which in turn increases the amount of information that can be reliably transmitted. For example, for $N = 32$, as P_S increases from 0 to 5 dBm, the ergodic capacity increases by 89.2 %. In addition, we observe that for a fixed P_S, as N increases, the ergodic capacity also increases. For instance, for $P_S = 5$ dBm, as N changes from 32 to 64, the ergodic capacity increases by 69.64%.

Similarly, Fig. 4 illustrates the ergodic capacity of the double-RIS system with varying N,$\beta = 1$, and $\Omega = 1$.
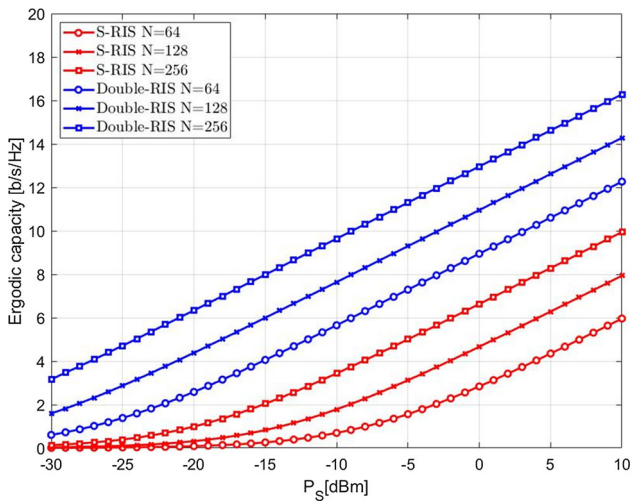
Fig. 5 Ergodic Capacity Comparison of S-RIS and double-RIS system versus transmit power of the source (P_S) for varying N, $\beta = 1$ and $\Omega = 1$

Fig. 6 Simulated Ergodic Capacity of S-RIS and double-RIS system versus transmit power of the source (P_S) for varying β, $N = 32$ and $\Omega = 1$

Similar to the S-RIS system we observe an increase in the ergodic capacity as P_S increases for fixed N and for fixed P_S, ergodic capacity increases with N for fixed P_S, as N doubles, we observe an improvement of 2 b/s/Hz in EC for S-RIS and double RIS systems. Finally, from Figs. 3 and 4, we observe the tightness of upper and lower bounds as the value of N increases which indicates the accuracy of closed-form expressions (C_{ub_n}, C_{lb_n}) derived in previous section.

Figure 5 compares the ergodic capacity of S-RIS and double-RIS systems for varying N by fixing the Weibull shape and scale parameters equal to 1. Double-RIS system shows significant improvement in ergodic capacity with the same number of reflecting elements for a fixed P_S. For instance, when P_S is fixed at 5 dBm double-RIS system with $N = 32$ shows an improvement of 6 b/s/Hz over the S-RIS system with $N = 32$. Finally, it is observed that when P_S is varying from -30 dBm to 10 dBm for a double RIS-system with $N = 64$, shows an approximate improvement of 0.5 to 2 b/s/Hz over an S-RIS system with $N = 256$.

Figure 6 shows the impact of Weibull shape parameter β on the ergodic capacity of S-RIS and double-RIS systems for $N = 32$ and $\Omega = 1$. As mentioned in the previous section, fading severity decreases with an increase in β. Consistent with this, the results indicate that increasing β leads to an increase in the ergodic capacity of the system. As can be seen, for a fixed β as, P_S increases the ergodic capacity increases monotonically. It is worth noting that $\beta = 2$ corresponds to the Rayleigh fading scenario, which is a special case of the Weibull distribution.

In Fig. 7, we compare the outage probability of both systems with $\beta = 1$ and $\Omega = 1$. It can be inferred from Fig. 7 that the theoretical results match with simulation counterparts. As expected, in both systems, for a fixed N, as P_S increases, we
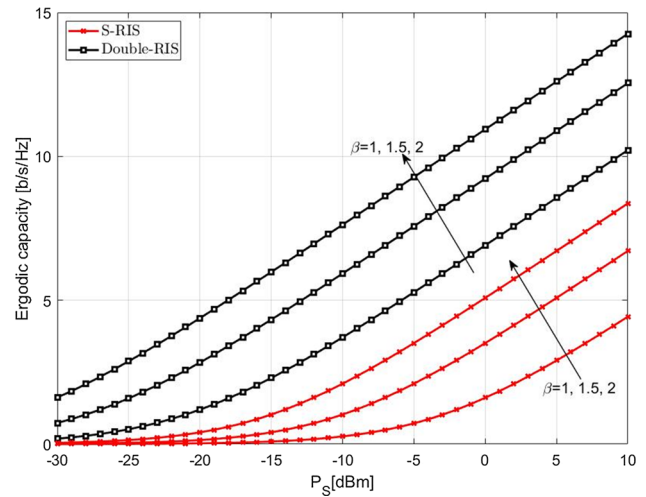
observe sharp decrease in outage probability. For example, for $N = 64$, OP decreases by 10 times as P_S changes from 5 to 6 dBm in S-RIS system whereas in double-RIS system, for $N = 64$, OP decreases by 10 times as P_S changes from -11 to -10 dBm. In addition, the rate of decrease is faster with a larger N.

Figure 8 shows the impact of Weibull shape parameter β on the outage probability of S-RIS and double-RIS system for $N = 32$ and $\Omega = 1$, where $\beta = 2$ denotes the Rayleigh fading. For fixed P_S, we observe an improvement in the outage probability as β increase. In addition, we observe that for a fixed β as, P_S increases the outage probability decreases at faster rate.

In Fig. 9, taking the total power consumed by the source, destination nodes and RIS elements into account, we evaluate the energy efficiency (EE) of the S-RIS and double-RIS systems as a function of target spectral efficiency (R). The EE of a RIS-aided system can be defined as $EE = BW_T \times R/P_{Total}$ [Mbit/Joule] [4], P_{Total} is the total power consumed by the system and calculated as, $P_{Total} = P_S + NP_i + P_c^S + P_c^D$. Double-RIS system shows higher energy efficiency than the S-RIS system. When $R \leq \widetilde{R} = 17.5$ b/s/Hz, the double-RIS system with $N = 64$ surpasses system with $N = 128$ in terms of EE. Similarly, when $R \leq \widetilde{R} = 12.5$ b/s/Hz, S-RIS system with $N = 64$ achieves higher energy efficiency system with $N = 128$ where $\widetilde{R}$ is the transition point as indicated in Fig. 9. The above phenomenon is due to the fact that, the P_{Total} increases linearly and R increases logarithmically with N.

The same can be observed from Table 2. For instance, when the target SE is $R=4$, D-RIS system can enhance the EE 94 by up to 94.65% and 96.23% for $N=64$ and $N=128$ respectively compared to S-RIS system. Similarly, for $R=6$,

Fig. 7 Outage probability comparison of S-RIS and double-RIS system versus transmit power of the source (P_S) for varying N, $\beta = 1$ and $\Omega = 1$
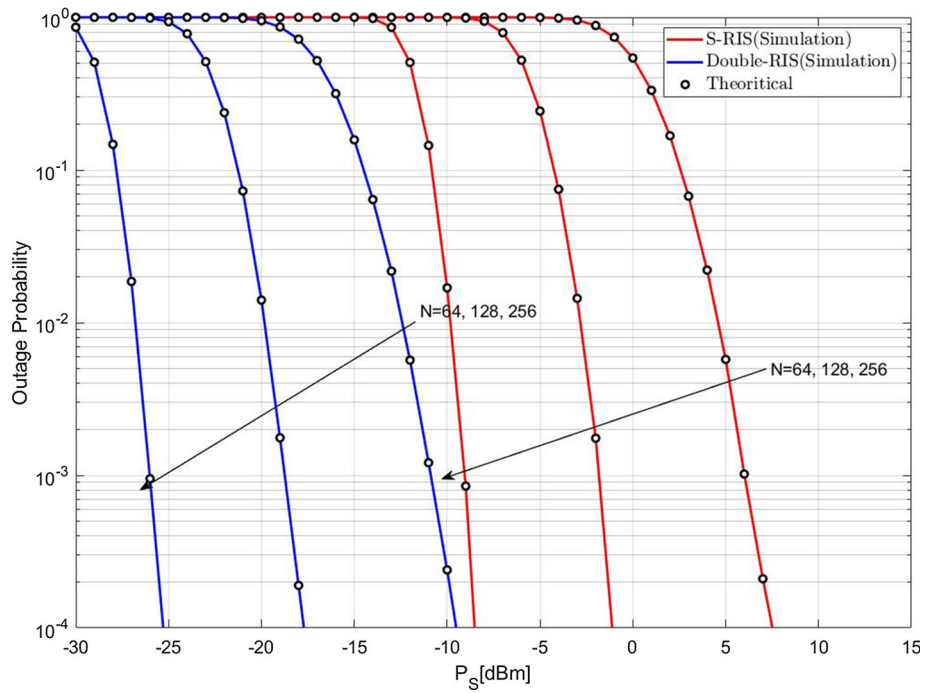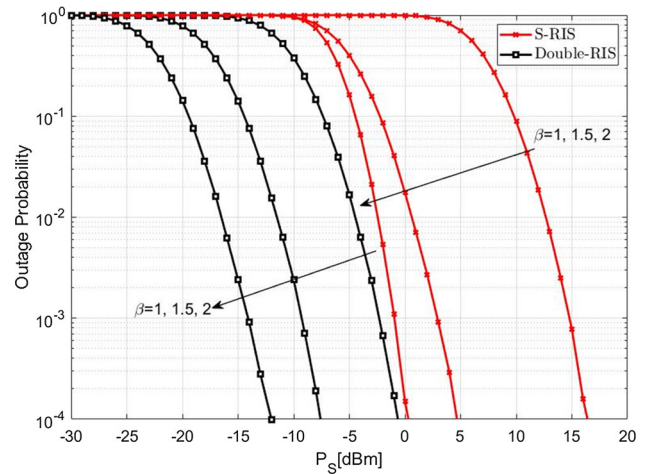

Fig. 8 Outage Probability of S-RIS and double-RIS system versus transmit power of the source (P_S) for varying β, $N = 32$ and $\Omega = 1$

D-RIS system can enhance the EE by up to 100.16% and 114.21% for N=64 and N=128 respectively compared to S-RIS system.

5 Impact of RISs location on the ergodic capacity and energy efficiency

To gain further insights about the considered system we compared the proposed D-RIS system with S-RIS system by varying the location of RISs and analyzed the ergodic capacity and energy efficiency.

Figure 10 depicts the impact of changing the horizontal distance $x_R \in (0, 200)$ on the ergodic capacity. In S-RIS system, we observed the improved performance in ergodic capacity when RIS is in the vicinity of either source or destination node when varying the position of RIS since the double fading problem is minimum which is directly proportional to the product of $d_{SR} = \sqrt{x_R{}^2 + y_R{}^2}$ and $d_{RD} = \sqrt{(d_{SD} - x_R)^2 + y_R{}^2}$. Similarly, for the proposed D-RIS system we simulated the ergodic capacity by changing the location of RIS' for two different scenarios without altering the far-field assumption: (i) R_1 and R_2 placed closer to the S and D, (ii) R_1 and R_2 placed midway between the S and D. From the figure it is observed that the proposed D-RIS system $\left((x_{R_1}, y_{R_1}) = (5, 10), (x_{R_2}, y_{R_2}) = (195, 10)\right)$ outperforms the S-RIS system in terms of ergodic capacity but when the single RIS is placed nearer to S or D, it achieves

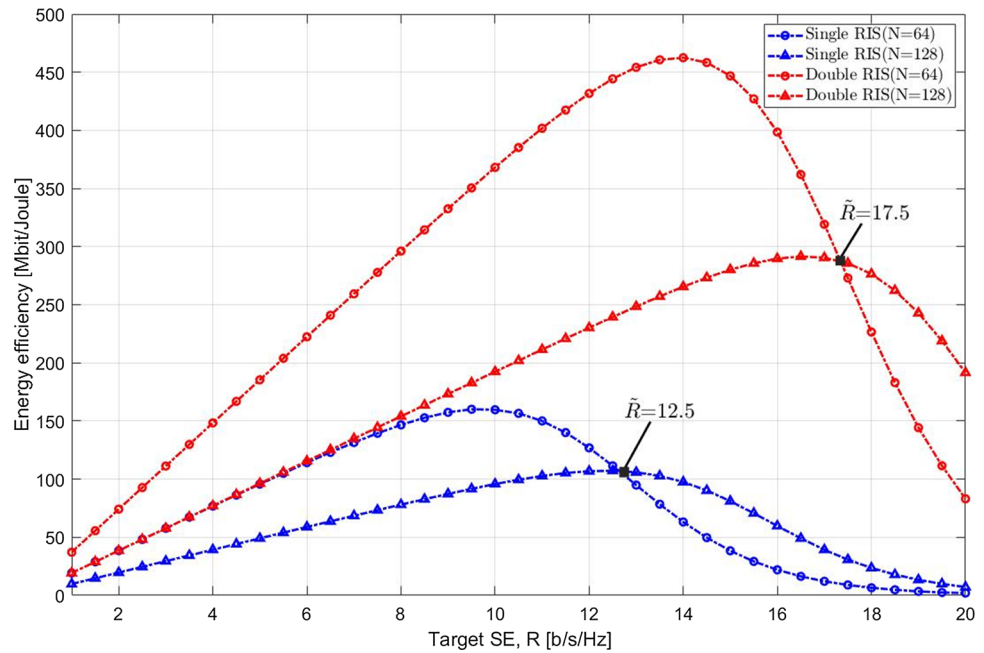**Fig. 9** The energy efficiency of S-RIS and double-RIS system as a function of target SE (R)

Table 2 Evaluation metrics

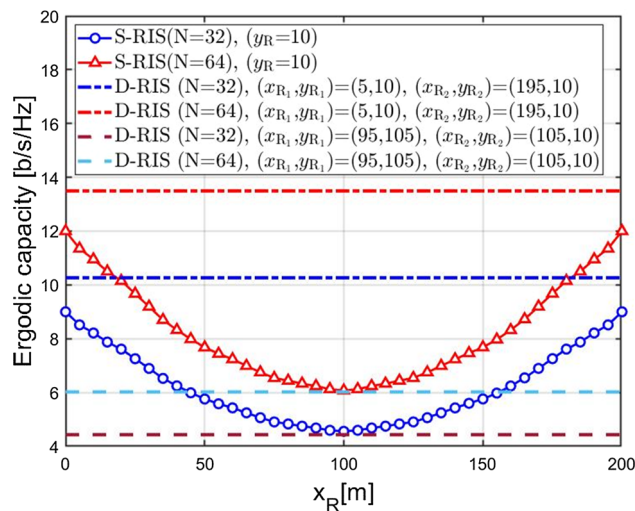| Target SE, R (b/s/Hz)	S-RIS system			Double-RIS system	
	N	P_S required (mW) to achieve Target SE	EE (Mbit/Joule)	P_S required (mW) to achieve Target SE	EE (Mbit/Joule)
4	64	1.54	76.81	0.025	148.35
	128	0.38	39.26	0.006	77.04
6	64	6.45	114.14	0.100	222.46
	128	1.58	53.94	0.031	115.55

Fig. 10 Impact of location of RISs on Ergodic capacity of the S-RIS and D-RIS system for varying N, $\beta = 1, \Omega = 1$ and $P_S = 10 dBm$

high ergodic capacity compared to that of the D-RIS system $\left((x_{R_1}, y_{R_1}) = (95, 10), (x_{R_2}, y_{R_2}) = (105, 10) \right)$.

In Fig. 11, we analyze the EE of S-RIS system by placing the RIS nearer to the S, D, and middle of S-D link, and compare it with two different scenarios of D-RIS system. From Figs. 9 and 11 it is observed, that the S-RIS system with RIS placed either near to S or D achieved same ergodic performance and energy efficiency which outperforms the S-RIS system with RIS placed in the middle S-D link and D-RIS system of scenario (ii). However, the proposed D-RIS system with R_1 and R_2 placed near to source and destination respectively, shown superior performance than the above mentioned systems with same number of reflecting elements. Figures 10 and 11 clearly reveal that D-RIS with optimally positioned RISs outperforms S-RIS system with same number of reflecting elements. Thus, the positioning of RISs in a D-RIS or multiple-RIS is an important factor in optimizing the performance gains.

Fig. 11 Impact of RISs location on the energy efficiency of S-RIS and double-RIS system as a function of target SE (R) for $N = 64$, $\beta = 1$, $\Omega = 1$
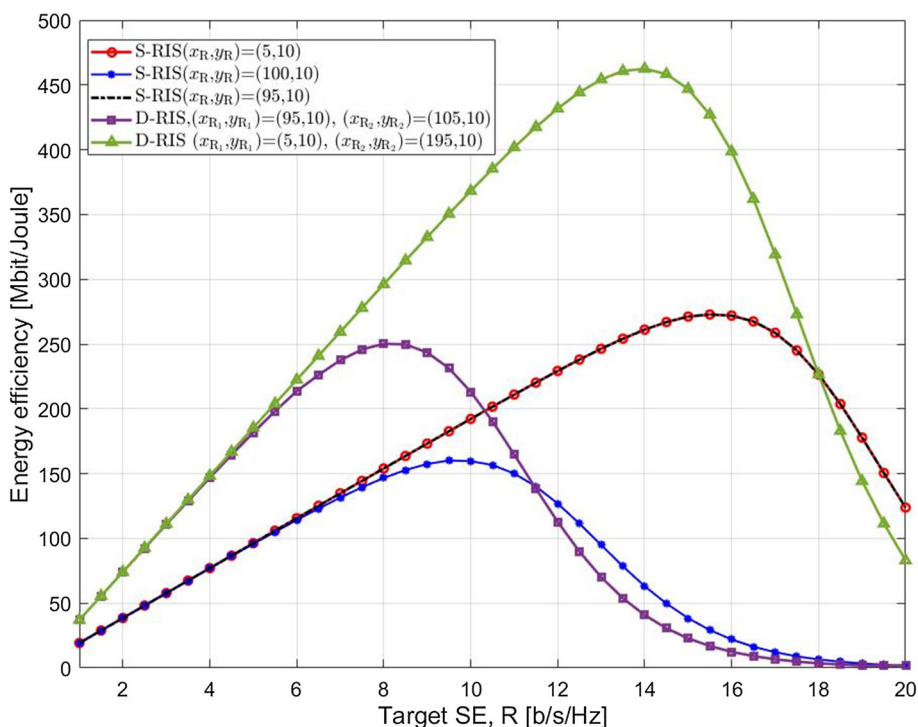
6 Conclusion

In this paper, we analyze the ergodic capacity and outage probability of single-RIS, double-RIS assisted systems over Weibull fading channels. Relying on central limit theorem, we derive the statistical parameters such as mean, variance and second order moment of received SNR for both systems. Thereby, we derived the closed-form expression for the lower, upper bounds of ergodic capacity and outage probability. The theoretical results are validated through Monte-Carlo simulations with various system parameters and found that the bounds are tight for larger number of reflecting elements. In addition, we compare the performance of both systems with equal number of reflecting elements and found that the proposed double-RIS system with R_1 and R_2 placed near to source, and destination respectively outperforms the S-RIS system. Also, we provide the energy efficiency analysis as a function of required spectral efficiency, from the analysis we found that, double-RIS assisted systems is energy-efficient than single-RIS. At the end we simulate the impact of RISs placement on the ergodic capacity of double-RIS system in comparison with the single-RIS system. Finally, we conclude that instead of deploying single RIS in the midway between source–destination link, placing two RIS, in the vicinity of source and destination with overall number of reflecting elements equal to single-RIS is an energy-efficient solution to improve the overall performance. It is worth noting that the EE of the systems will mainly depend on the target SE (R), number of reflecting elements (N) and location of the RIS.

Hence, the D-RIS system that switches between single-RIS and double-RIS modes can help to minimize transmit power and maximize EE, especially in cases where the target SE is not too high. Evaluating the performance of the proposed system when transceivers are in the near-field regime of RISs with appropriate channel models can be considered as future works.

Declarations

Appendix A

As mentioned earlier $\gamma_{D,1}$ follows NCCS with following mean, variance and second order moment [24],

$$\mathbb{E}\big[\gamma_{D,1}\big] = \sigma_{Z_1}^2 + \lambda_{Z_1}{}^2, \tag{24}$$

$$\mathbb{V}ar\big[\gamma_{D,1}\big] = 2\sigma_{Z_1}^4 + 4\sigma_{Z_1}^2\lambda_{Z_1}{}^2, \tag{25}$$

$$\mathbb{E}\left[\gamma_{D,1}{}^2\right] = \mathbb{V}ar\left[\gamma_{D,1}\right] + \mathbb{E}\left[\gamma_{D,1}\right]^2$$
$$= 3\sigma_{Z_1}^4 + 6\sigma_{Z_1}^2 \lambda_{Z_1}{}^2 + \lambda_{Z_1}{}^4, \tag{26}$$

where $\lambda_{Z_1} = \sqrt{\left(N_S \Omega^{\frac{2}{\beta}}(\Gamma(1+1/\beta))^2\right)^2}$ is non-centrality parameter, and $\sigma_{Z_1}^2 = N_S \Omega^{\frac{4}{\beta}}((\Gamma(1+2/\beta))^2 - \Gamma((1+1/\beta))^4)$. By substituting λ_{Z_1}, $\sigma_{Z_1}^2$ in Eq. (24)–(26) and after some algebraic calculations we will get mean, second order moment and variance of $\gamma_{D,1}$ as in Eq. 9(a)–(c).

Similarly, by substituting non-centrality parameter $\lambda_{Z_2} = \sqrt{\left(2N_D \Omega^{\frac{2}{\beta}}(\Gamma(1+1/\beta))^2\right)^2}$ and $\sigma_{Z_2}^2 = 2N_D \Omega^{\frac{4}{\beta}}\left[(\Gamma(1+2/\beta))^2 - (\Gamma(1+1/\beta))^4\right]$ in Eq. (27)–(29) and after doing algebraic calculations we will get the mean, second order moment and variance of $\gamma_{D,2}$ as in Eq. 12(a)–(c).

$$\mathbb{E}\left[\gamma_{D,2}\right] = \sigma_{Z_2}^2 + \lambda_{Z_2}{}^2, \tag{27}$$

$$\mathbb{V}ar\left[\gamma_{D,2}\right] = 2\sigma_{Z_2}^4 + 4\sigma_{Z_2}^2 \lambda_{Z_2}{}^2, \tag{28}$$

$$\mathbb{E}\left[\gamma_{D,2}{}^2\right] = \mathbb{V}ar\left[\gamma_{D,2}\right] + \mathbb{E}\left[\gamma_{D,2}\right]^2$$
$$= 3\sigma_{Z_2}^4 + 6\sigma_{Z_2}^2 \lambda_{Z_2}{}^2 + \lambda_{Z_2}{}^4. \tag{29}$$

References

1. Di Renzo, M., et al. (2020). Smart radio environments empowered by reconfigurable intelligent surfaces: How it works, state of research, and the road ahead. *IEEE Journal on Selected Areas in Communications, 38*(11), 2450–2525. https://doi.org/10.1109/JSAC.2020.3007211

2. Basar, E., Di Renzo, M., De Rosny, J., Debbah, M., Alouini, M.-S., & Zhang, R. (2019). Wireless communications through reconfigurable intelligent surfaces. *IEEE Access, 7*, 116753–116773. https://doi.org/10.1109/ACCESS.2019.2935192

3. Boulogeorgos, A. A., & Alexiou, A. (2020). Performance analysis of reconfigurable intelligent surface-assisted wireless systems and comparison with relaying. *IEEE Access, 8*, 94463–94483. https://doi.org/10.1109/ACCESS.2020.2995435

4. Björnson, E., Özdogan, Ö., & Larsson, E. G. (2020). Intelligent reflecting surface versus decode-and-forward: How large surfaces are needed to beat relaying? *IEEE Wireless Communications Letters, 9*(2), 244–248. https://doi.org/10.1109/LWC.2019.2950624

5. Du, L., Zhang, W., Ma, J., & Tang, Y. (2021). Reconfigurable intelligent surfaces for energy efficiency in multicast transmissions. *IEEE Transactions on Vehicular Technology, 70*(6), 6266–6271. https://doi.org/10.1109/TVT.2021.3080302

6. Huang, C., Zappone, A., Alexandropoulos, G. C., Debbah, M., & Yuen, C. (2019). Reconfigurable intelligent surfaces for energy efficiency in wireless communication. *IEEE Transactions on Wireless Communications, 18*(8), 4157–4170.

7. You, L., Xiong, J., Ng, D. W. K., Yuen, C., Wang, W., & Gao, X. (2020). Energy efficiency and spectral efficiency tradeoff in ris-aided multiuser MIMO uplink transmission. *IEEE Transactions on Signal Processing, 69*, 1407–1421.

8. Tan, F., Xu, X., Chen, H., & Li, S. (2023). Energy-efficient beamforming optimization for MISO communication based on reconfigurable intelligent surface. *Physical Communication, 57*, 4–11. https://doi.org/10.1016/j.phycom.2022.101996

9. Yang, L., Yang, Y., Hasna, M. O., & Alouini, M.-S. (2020). Coverage, Probability of SNR gain, and DOR analysis of RIS-aided communication systems. *IEEE Wireless Communications Letters, 9*(8), 1268–1272. https://doi.org/10.1109/LWC.2020.2987798

10. Kumar, S., Yadav, P., Kaur, M., & Kumar, R. (2022). A survey on IRS NOMA integrated communication networks. *Telecommunication Systems, 80*(2), 277–302. https://doi.org/10.1007/s11235-022-00898-y

11. Shambharkar, D., Dhok, S., Singh, A., & Sharma, P. K. (2022). Rate-splitting multiple access for RIS-aided cell-edge users with discrete phase-shifts. *IEEE Communications Letters*. https://doi.org/10.1109/LCOMM.2022.3195199

12. Do, T. N., Kaddoum, G., Nguyen, T. L., da Costa, D. B., & Haas, Z. J. (2021). Multi-RIS-aided wireless systems: Statistical characterization and performance analysis. *IEEE Transactions on Communications, 69*(12), 8641–8658. https://doi.org/10.1109/TCOMM.2021.3117599

13. Yang, L., Yang, Y., da Costa, D. B., & Trigui, I. (2021). Outage probability and capacity scaling law of multiple RIS-aided networks. *IEEE Wireless Communications Letters, 10*(2), 256–260. https://doi.org/10.1109/LWC.2020.3026712

14. Yang, Z., et al. (2022). Energy-efficient wireless communications with distributed reconfigurable intelligent surfaces. *IEEE Transactions on Wireless Communications, 21*(1), 665–679. https://doi.org/10.1109/TWC.2021.3098632

15. Aung, P.S., Kyaw Tun, Y., Han, Z., Hong, C.S. (2022). Energy-efficiency maximization of multiple RISs-enabled communication networks by deep reinforcement learning, In ICC 2022 - IEEE International conference on communications, Seoul, Korea, Republic of, pp. 2181–2186, doi: https://doi.org/10.1109/ICC45855.2022.9838468.

16. Han, Y., Zhang, S., Duan, L., & Zhang, R. (2020). Cooperative double-irs aided communication: Beamforming design and power scaling. *IEEE Wireless Communications Letters, 9*(8), 1206–1210. https://doi.org/10.1109/LWC.2020.2986290

17. Dong, L., Wang, H.-M., Bai, J., & Xiao, H. (2021). Double intelligent reflecting surface for secure transmission with inter-surface signal reflection. *IEEE Transactions on Vehicular Technology, 70*(3), 2912–2916. https://doi.org/10.1109/TVT.2021.3062059

18. Yildirim, I., Uyrus, A., & Basar, E. (2021). Modeling and analysis of reconfigurable intelligent surfaces for indoor and outdoor applications in future wireless networks. *IEEE Transactions on Communications, 69*(2), 1290–1301. https://doi.org/10.1109/TCOMM.2020.3035391

19. Zheng, B., & Zhang, R. (2020). Intelligent reflecting surface-enhanced OFDM: Channel estimation and reflection optimization. *IEEE Wireless Commun. Lett., 9*(4), 518–522.

20. Alwazani, H., Nadeem, Q.U.A., & Chaaban, A. (2020). Channel estimation for distributed intelligent reflecting surfaces assisted multi-user MISO systems, In Proc. IEEE Globecom Workshops, December, pp. 1–6.

21. Alnwaimi, G., & Boujemaa, H. (2021). Optimal packet length for wireless communications using reconfigurable intelligent surfaces. *Telecommunication Systems, 77*(4), 683–696. https://doi.org/10.1007/s11235-021-00783-0

22. Sagias, N. C., Zogas, D. A., Karagiannidis, G. K., & Tombras, G. S. (2004). Channel capacity and second-order statistics in Weibull

fading. *IEEE Communications Letters, 8*(6), 377–379. https://doi.org/10.1109/LCOMM.2004.831319

23. Sagias, N. C., & Tombras, G. S. (2007). On the cascaded Weibull fading channel model. *Journal of the Franklin Institute, 344*(1), 1–11. https://doi.org/10.1016/j.jfranklin.2006.07.004

24. Proakis, J. G. (2008). *Digital communications* (5th ed.). McGraw-Hill.

25. Zhang, Q., Jin, S., Wong, K.-K., Zhu, H., & Matthaiou, M. (2014). Power scaling of uplink massive MIMO systems with arbitrary-rank channel means. *IEEE Journal of Selected Topics in Signal Processing, 8*(5), 966–981. https://doi.org/10.1109/JSTSP.2014.2324534

26. Hashemi, R., Ali, S., Mahmood, N. H., & Latva-aho, M. (2021). Average rate and error probability analysis in short packet communications over RIS-aided URLLC systems. *IEEE Transactions on Vehicular Technology, 70*(10), 10320–10334. https://doi.org/10.1109/TVT.2021.3105878

27. Annamalai, A., Tellambura, C., & Matyjas, J. (2009). A new twist on the generalized marcum Q-function QM(a, b) with Fractional-order M and its applications, In 2009 6th IEEE consumer communications and networking conference, 2009, pp. 1–5, doi: https://doi.org/10.1109/CCNC.2009.4784840.

V. Nivetha received her B.E. degree in Electronics and Communication Engineering from Anna University, India, in 2015, and her M.E. degree in Communication Systems from the College of Engineering, Guindy, Anna University, India in 2019. She is currently pursuing Ph.D. degree in Electronics and Communication Engineering from National Institute of Technology, Tiruchirappalli, India. Her current research interests include multicarrier modulation for future wireless systems.

V. Sudha received her B.E degree in Electronics and Communication Engineering from Bharathidasan University, India in 2000 and the M.E degree in Communication Systems from Anna University, India in 2006. She completed her Ph.D. in the area of wireless communication systems at National Institute of Technology, Tiruchirappalli in 2017. She has 22 years of teaching experience. Currently, she is working as Associate Professor in the Department of Electronics and Communication Engineering, National Institute of Technology (NIT), Tiruchirappalli, India. Her research interests include Multicarrier Wireless Systems, Digital Communication, Wireless Optical Communication, Wireless Networks. She has published several papers in International Journals and Conferences. She is a life member of ISTE.

R. Mahammad Rafi received his B.Tech degree in Electronics and Communication Engineering from Jawaharlal Nehru Technological University, Anantapur, India in 2013 and the M.Tech degree in Communications and Signal Processing from Jawaharlal Nehru Technological University, Anantapur, India in 2016. He is currently working towards his Ph.D. degree in National Institute of Technology (NIT), Tiruchirappalli, Tamilnadu, India from 2019. His research interests include mmWave communication, reconfigurable intelligent surface, and channel modeling.